IL NUOVO CIMENTO **48 C** (2025) 54
DOI 10.1393/ncc/i2025-25054-9

Colloquia: IWM-EC 2024

Clustering states investigation with FARCOS detectors

F. Risitano(1)(2)(*), B. Gnoffo(1)(3), M. Trimarchi(1)(2), L. Acosta(4)(5), G. Cardella(1), E. De Filippo(1), D. Dell'Aquila(6)(7), E. Geraci(1)(3), I. Lombardo(1)(3), C. Maiolino(8), N. S. Martorana(1), A. Pagano(1), E. V. Pagano(8), M. Papa(1), S. Pirrone(1), G. Politi(1)(3), L. Quattrocchi(1)(2), F. Rizzo(3)(8)(9), P. Russotto(8) and C. Zagami(3)(8)(9)

(1) *INFN, Sezione di Catania - Catania, Italy*
(2) *Dipartimento MIFT, Università di Messina - Messina, Italy*
(3) *Dipartimento di Fisica e Astronomia "E. Majorana", Università degli Studi di Catania Catania, Italy*
(4) *Instituto de Física, Universidad Nacional Autónoma de México - Mexico City, Mexico*
(5) *Instituto de Estructura de la Materia, CSIC - Madrid, Spain*
(6) *Dipartimento di Fisica "E. Pancini", Università degli Studi di Napoli Federico II Napoli, Italy*
(7) *INFN, Sezione di Napoli - Napoli, Italy*
(8) *INFN-LNS - Catania, Italy*
(9) *Centro Siciliano di Fisica Nucleare e Struttura della Materia - Catania, Italy*

received 26 November 2024

Summary. — The FARCOS array is a compact and innovative detection system, built for studies of spectroscopy, femtoscopy and correlations, offering high energy and angular resolution. At INFN-LNS, an experiment was performed to study the cluster structure of light radioactive nuclei, such as ^{10}Be, ^{13}B and ^{16}C, using the CHIMERA and FARCOS multidetector. The four FARCOS detectors were placed at small angle for an in depth study of the correlation of break-up fragments resulting from the decay of excited cluster states. An overview of the analysis still in progress will be given, showing, in particular, some results for the analysis of ^{10}Be clustering.

1. – Introduction

The balancing of the internal nuclear and Coulombian forces of a nucleus can lead to the formation of interesting aggregation phenomena of nucleons, referred to as *clusters* [1, 2]. The formation of such structures is an intriguing topic of study in modern nuclear physics and it is an excellent tool for better understanding the behavior of nuclear forces, especially under extreme conditions. Particularly interesting is the formation of cluster structures of α particles, significant for their internal stability [3]. In fact, there

(*) E-mail: `farisitano@unime.it`; `fabio.risitano@ct.infn.it`

are several cases of α cluster structures in self-conjugated nuclei (^{8}Be, ^{12}C, ^{16}O, ^{20}Ne,...). The addition of neutrons to such systems amplifies the effect of the formation of clustering state, allowing for new excited states and structures [4]. In this case, similarly to molecular chemical bonds, we speak of valence neutrons, behaving in a similar way to the electrons exchanged in covalent molecular bonds. Understanding the effect of valence neutrons on the formation of cluster states, especially as a function of the excitation energy of the nucleus, is a benchmark for our knowledge of the nuclear force. Although various theoretical models explain and predict the existence of different cluster states for different ionic species, their experimental investigation still has a long way to go. Along this line of research, experiments were performed at Laboratori Nazionali del Sud of INFN aiming to study cluster states in various neutron-rich radioactive species, particularly those that may exhibit molecular or exotic cluster states, like ^{10}Be, ^{13}B and ^{16}C [5-7]. An exemplary case is the cluster structure of neutron-rich isotopes of beryllium. While ^{8}Be exhibits an unstable cluster state at the ground state, the addition of neutrons allows the formation of molecular cluster states of α particles [8]. The case of ^{10}Be is also currently still under study, exhibiting multiple rotational bands and in particular a large moment of inertia band in the α:2n:α configuration [5,9] and moreover, at much higher energies, the band-terminating states belonging to this rotational band are still not fully understood. In this work, the main results of the ongoing analysis of ^{10}Be spectroscopy, using the FARCOS telescopes and the invariant mass technique will be presented.

2. – Experimental details

Aiming to study cluster states in neutron-rich light ions, such as molecular states of ^{10}Be and ^{16}C and exotic cluster structures in ^{13}B, an experiment was performed at INFN-LNS by using four FARCOS telescopes coupled with CHIMERA. CHIMERA [10] is a 4π multidetector made of 1192 independent two-stage Si-CsI(Tl) telescopes arranged in 9 forward rings and a sphere, covering almost the entirety of the 4π solid angle. A single FARCOS array consists of three different stages [11]. The first two stages are Double Sided Silicon Strip Detectors (DSSSDs), 300 and 1500 μm thick, respectively. Each DSSSD is made of 32 strips of 2 mm pitch, on both the front and back sides, granting a total active area of $64 \times 64\,\mathrm{mm}^2$. The third stage is made by four CsI(Tl) scintillators, each one 6 cm thick, readout by a photodiode. In its entirety, a single FARCOS telescope grants of a total of 132 different and independent channels, offering the possibility of acquiring a high signal density for a small active surface. Thanks to its three stages, a variety of techniques of detection and identification can be used depending on the energy of the incident ions [12]: it can be used for studies of isospin physics at intermediate energy and also at lower energies for research of fusion or astrophysical interests [13]. Furthermore, thanks to the 32 strip grid on the front and back sides, by accurately measuring the angular position of each virtual "pixel" with respect to the beam axis, it is possible to obtain a high angular resolution, especially crucial for the study of cluster structures. In the case of the present experiment, the four FARCOS telescopes were placed at small angles, between the rings of CHIMERA and the sphere, covering polar angles in the range $2.2^{\circ} \leq \theta \leq 8.8^{\circ}$ at about 75 cm from the reaction target (CH_2 polyethylene). The experiment was conducted using a radioactive beam produced by the FRIBs (In-Flight Radioactive Ion Beams) facility at the LNS [14,15]. By accelerating a primary beam of ^{18}O using the LNS Superconducting Cyclotron and fragmenting it on a beryllium target placed along the beamline, a cocktail beam containing various ionic species was produced. To identify the incident ions in the beam event-by-event, a tagging system based on the ΔE-ToF technique was employed [16], consisting of a Microchannel plate detector positioned upstream on the beamline and a DSSSD detector placed about 2 meters from the reaction target in the experimental hall. Correlating the time of flight between the two detectors and the energy loss on the downstream silicon detector, a distribution as in fig. 1 (left) was obtained, through which it is possible to identify all the distributions with different ion species of the cocktail beam, from ^{6}He to ^{17}C.

3. – Calibrations, data selection and cleaning of spurious events

An extensive work of calibrations was performed on the tagging system and FARCOS stages, for which new techniques have been studied to perform correct calibrations depending on the type of detector. As for the tagging system, after having produced a simulation of the radioactive beam production through the simulation software LISE++, it was possible to calibrate each of the DSSSD front and back strips both in time of flight and energy loss, correlating the experimental position in the channel of each isotopic distribution with the corresponding simulation. To calibrate the FARCOS array, different techniques have been used and developed specifically for this measurement and for its different stages [17], compared to those of other and more modern experiments that also used different electronics or digitized signals [12, 18, 19]. First, the 1500 μm DSSSD was calibrated on both sides, starting from the front one. To do this, ΔE-E matrices were produced for each front strip with the relative adjacent CsI. From each of these, it was possible to notice the presence of pronounced distributions at the end of each isotope ridge, signature of elastically scattered beams on hydrogen reaction target ions. It was then possible to use the energy loss of the elastic beams to calibrate each of the 32 strip fronts of the 1500 μm FARCOS detector stages. The DSSSD back side strips were instead calibrated by exploiting the main feature of silicon strip detectors: the energy lost of an incident ion passing through the layer of active material, is detected by the front and back side strips in the same way. Then, by correlating, strip by strip, the energy released on the front side strips calibrated through the previous method, with the non-calibrated back ones, a linear correlation matrix can be obtained, through which it is possible to extract a calibration line. An example can be seen on fig. 1 (right), showing the energy loss on a single back strip (abscissa), relative to the calibrated energy

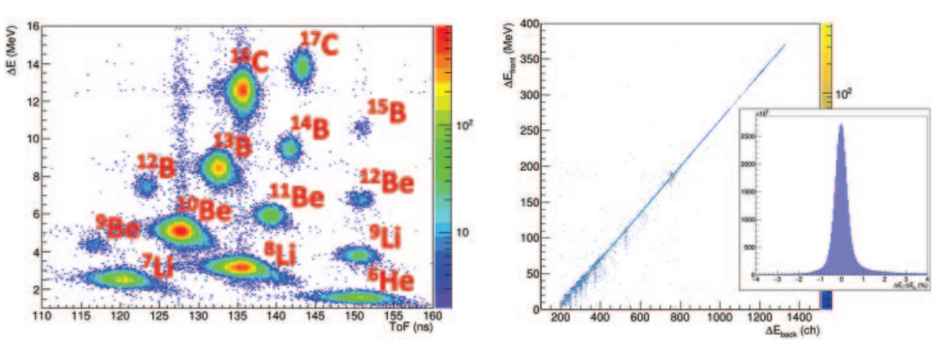

Fig. 1. – Left: tagging ΔE-ToF calibrated plot. Several isotopic species can be identified through simulations. Figure adapted from ref. [17]. Right: calibration matrix, obtained by plotting the uncalibrated signal of a back strip of a 1500 μm stage of a FARCOS detector *vs.* the front side calibrated signal. The profile of the linear trend is shown in small as a percentage difference.

obtained from all the adjacent front calibrated strips (ordinate). This method is also useful to check the validity of the calibrations: if one of them was even slightly wrong more correlation lines slightly shifted would appear on the matrix. For the CsI(Tl) calibration, the RNQM model was employed [17, 20], allowing to obtain a parametrization of the light emitted by a scintillator, for different charges, masses and energy ranges. Moreover, a code in the analysis was also implemented to identify event by event the impinging isotopes in charge and mass. One of the key aspects of the FARCOS array is that, thanks to its multitude of independent acquisition channels, it can be used even for measurements in which high multiplicity is required. Since each event is normally associated with a front and back strip, by appropriately measuring the polar angles of the 1024 virtual pixels of the DSSSDs, it is therefore possible to also have correlations at very small angles, thus offering a high angular resolution. In order to make the most of this quality of the FARCOS detectors, some filtering and selection techniques of the experimental data have been developed, in order to discard spurious events, increment the overall signal-to-noise ratio and associate to the incident ion the correct angles θ and ϕ, method usually defined as pixelation [19]. First a timing window was applied on the time of the signal, thus excluding events where it was detected incorrectly, allowing to remove considerable background noise. Furthermore, for DSSSDs, a coincidence window was applied between the two collected signals of the front and back sides, in order to reject events in which the temporal differences were too high, due for example to possible other spurious events. After applying this filter, an analysis was done on the correct assignment of the pixel. As mentioned above, each of the 32 front and back side channels are independent, so when there are multiple front and back side signals, it is necessary to understand which pixel a particle actually passed through. To do this, an algorithm was developed which, employing the previously mentioned principle of equality in the energy detected between the front and back sides, compares the energy detected on the front strips with each of the back strips. This is done by trying to minimize the squared difference $E_{diff}(j,k) = (E_j - E_k)^2$ with j and k the indices of the front and back strips respectively. In this way, whatever the multiplicity of the event, the most likely combination of front and back strip assignment is obtained. Furthermore, this method is also useful to identify and correct or discard spurious phenomena such as electromagnetic *inductions* or *interstrip* events [21]: in these cases, when an ion interacts with a strip, one of the lateral strips also fires up, therefore increasing the multiplicity and complicating the analysis. This occurs due to the interaction of the electromagnetic field of the main fired strip with a lateral strip, slightly delayed in time but still within the timing window discussed above. If the energy of the fired strip is consistent with that of the back, the event is collected while the inductively fired strip is discarded from the analysis. On the other hand, it is possible that an incident ion interacts in the area of oxide between two adjacent strips, with the result of losing energy in both strips. This event, thus called interstrip, is analyzed considering the sum of the two energies of the adjacent strips instead of taking them individually, and then comparing it with the event on the opposite face. This is based on the principle that the sum of the energy collected by the two adjacent strips is equal to the total energy lost by the ion, thus allowing the comparison with the energy collected by a single strip on the opposite face. A reasonable number of events have been identified and corrected using this method, although their energy resolution is indeed lower than single strip events.

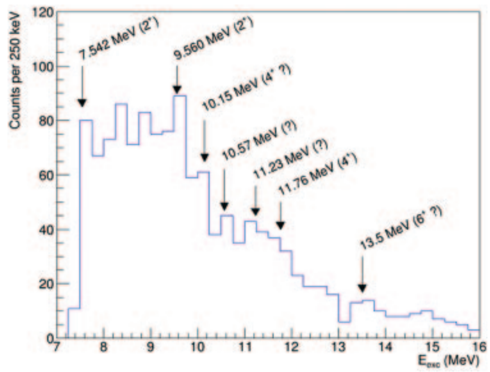

Fig. 2. – Excitation spectrum obtained for ^{10}Be reconstructed for the ^{6}He+^{4}He decay channel. Arrows indicate the position of peaks known in the literature. Brackets show the J^{π} spin parity value if known.

4. – Analysis

Work was carried out on the spectroscopy of ^{10}Be starting from the ^{6}He+^{4}He cluster break-up decay channel. First the ^{10}Be beam is selected from the bunch of the incident cocktail beam, through a graphic cut on the tagging matrix. Then, event of pairs of ^{4}He and ^{6}He, detected in coincidence by FARCOS telescopes, are selected. In particular, only correctly reconstructed events and therefore events in which the polar angles θ and ϕ are known were used. To reconstruct the excitation spectrum in the laboratory frame for the ^{10}Be parent ion, the relative energy between the two daughter nuclei was calculated, summed then to the threshold for the reaction of 7.408 MeV, shown in fig. 2. The arrows represent many excitation levels gathered from several works from the literature [5, 9, 22], and it is possible to see some peaks in agreement, even though the low statistics and resolution can be misleading. Simulations of break-up of ^{10}Be for the interested ^{6}He+^{4}He decay channel were performed to study the behavior of the spectrum in various conditions of energy and angular resolution. A beam energy of 57 MeV/u was set, coherently with the value obtained from the tagging system, decaying into 7 possible different excitation stages retrieved from the literature and NNDC [5,9,22], described as a Breit-Wigner function (fig. 3 (left)). The probability of every level was also weighted by an empirical decreasing exponential function. The effect of the presence of the FARCOS array was also introduced, both in terms of efficiency, considering the experimental geometric configuration, and errors on the detection energy and angular resolution. For each event, the decay of the parent ^{10}Be nucleus to one of the possible excited states, weighted by energy, is simulated with the resulting emission of the two daughter ions. If such ions are detected by the FARCOS array, their total energy is smeared through a Gaussian peak of width equal to its 2%, consistent with the resolution expected from CsI scintillators. Moreover, the dimension of the FARCOS pixels were also taken into account by first identifying the pixel hit by the single ion and then replacing its absolute angles θ and ϕ with those of the fired pixel. It was then noted that it is possible to divide the spectrum into two different components: events in which the daughter ^{6}He and ^{4}He ions arrive on the same FARCOS detector (so having a small relative emission angle), or events in which they arrive on different telescopes (large relative angle) as shown in fig. 3 (right). Comparing this with the same selection criteria applied on experimental data, it

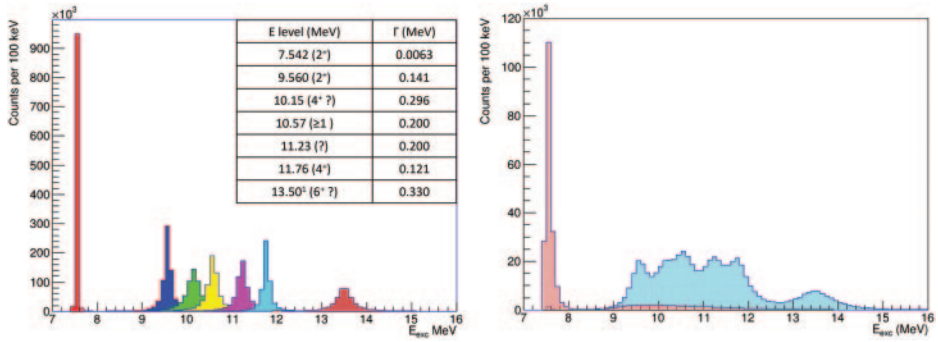

Fig. 3. – Left: simulation of the excitation energy spectrum of the ^{10}Be decay reconstructed from the clusters break-up products ^{6}He+^{4}He. Each peak corresponds to a different level (from the table). Right: same simulation as in the left side, with a distinction between events arriving on the same (red histogram) or on different FARCOS telescopes (blue histogram), in which a correction on the detection angle of the daughter ion and a Gaussian smearing to their total energy are applied (see text).

is possible to notice similar distributions. In particular for the first one, as in fig. 4, the presence of a peak at 7.6 MeV can be noticed, consistent with the one simulated with spin 2^+. On the other side, the shift to the right and the widening of the peak are caused by background and small errors in the measurement of the experimental pixel angles. In the future this issue will be addressed by measuring the detection angles through a laser system. Figure 4 (right) shows the spectrum obtained selecting events in which break-up fragments ^{6}He and ^{4}He hit two different telescopes. The presence of the first four peaks is seen, while probably the presence of a small shoulder of the 11.76 MeV peak can be observed. There still is some background noise, especially at low energy, between 8 and 9 MeV, and between 12 and 13 MeV, which worsens the observation of the not entirely clear peak at 13.5 MeV, previously predicted by other experiments at LNS performed by the CHIMERA Collaboration [5] and further measurements [2]. Improvements will regard in particular the cleaning and evaluation of background, while also increasing the

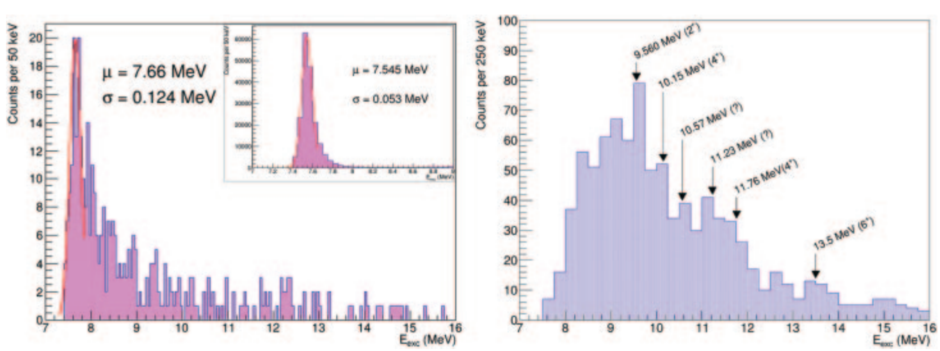

Fig. 4. – Left: selection of events where both daughter ions arrive at the same telescope (small relative emission angle), compared to the same selection of events in the simulation. Right: selection of events where the daughter particles arrive at different telescopes.

statistics by including the CHIMERA multidetector, which at this stage of the analysis was not considered and will probably give more information on the scattering of the recoil target.

5. – Conclusions

Investigations on cluster states using the FARCOS array is possible with noticeable results. Calibration and data filtering techniques for the collected data have been exposed, in particular highlighting the different techniques used depending on the type of detector. Particular attention was also given to the correct attribution of the pixel, and therefore of the polar angles of the interacting ions, independently from the multiplicity of the event. Some results on ^{10}Be spectroscopy for the ^{6}He+^{4}He cluster break-up channel have then been shown. An excitation spectrum was produced, in which it is possible to note the presence of various peaks of interest. In particular, a simulation of the decay of ^{10}Be from some excited states of interest was also produced, from which it is possible to observe the presence of two distinct components, at small and large relative angles between the produced fragments. This effect highlights the quality of the measurement especially at small angles, possible only thanks to the presence of the FARCOS array. In the future, the measurement of cluster states in radioactive ions will be further improved, including not only the multidetector CHIMERA, but also the innovative neutron detector NARCOS, currently under development [23-25].

REFERENCES

[1] Freer M. *et al.*, *J. Phys.: Conf. Ser.*, **381** (2012) 012009.
[2] Gnoffo B. *et al.*, *Front. Phys. Sect. Nucl. Phys.*, **10** (2022) 1061633.
[3] Lombardo I. and Dell'Aquila D., *Riv. Nuovo Cimento*, **46** (2023) 521.
[4] von Oertzen W., Freer M. and Kanada-En'yo Y., *Phys. Rep.*, **432** (2006) 43.
[5] Dell'Aquila D. *et al.*, *Phys. Rev. C*, **93** (2016) 024611.
[6] Risitano F. *et al.*, *Nuovo Cimento C*, **45** (2022) 60.
[7] Risitano F. *et al.*, *Nuovo Cimento C*, **47** (2024) 43.
[8] Kanada-En'yo Y. *et al.*, *Phys. Rev. C*, **102** (2020) 014607.
[9] Upadhyayula S. *et al.*, *Phys. Rev. C*, **101** (2020) 034604.
[10] Pagano A. *et al.*, *Nucl. Phys. A*, **704** (2004) 504.
[11] Pagano E. V. *et al.*, *EPJ Web of Conferences*, **117** (2016) 10008.
[12] Cardella G. *et al.*, *Eur. Phys. J. Plus*, **138** (2023) 89.
[13] Broggini C. *et al.*, *Riv. Nuovo Cimento*, **42** (2019) 103.
[14] Russotto P. *et al.*, *J. Phys.: Conf. Series*, **1014** (2018) 012016.
[15] Martorana N. S. *et al.*, *Nuovo Cimento C*, **45** (2022) 63.
[16] Lombardo I. *et al.*, *Nucl. Phys. B*, **215** (2021) 272.
[17] Risitano F. *et al.*, *J. Phys.: Conf. Ser.*, **2619** (2023) 012013.
[18] Acosta L. *et al.*, *2019 IEEE Nuclear Science Sympoisum and Medical Imaging Conference Proceedings* (IEEE) 2019, pp. 1–4.
[19] Cardella G. *et al.*, to be published in *Nucl. Instrum. Methods Phys. Res. A*, (2024).
[20] Parlog M. *et al.*, *Nucl. Instrum. Methods Phys. Res. A*, **482** (2002) 693.
[21] Acosta L. *et al.*, *IEEE Nuclear Science Symposium Conference Record* (IEEE) 2012, p. 1358.
[22] Tilley D. R. *et al.*, *Nucl. Phys. A*, **745** (2004) 155.
[23] Pagano E. V. *et al.*, *Front. Phys. Sect. Nucl. Phys.*, **10** (2023) 1051058.
[24] Pagano E. V. *et al.*, *Nucl. Instrum. Methods Phys. Res. A*, **889** (2018) 83.
[25] Pagano E. V. *et al.*, *Nucl. Instrum. Methods Phys. Res. A*, **1064** (2024) 169425.